Computers and Mathematics with Applications 58 (2009) 1055–1061

Contents lists available at ScienceDirect

Computers and Mathematics with Applications

journal homepage: www.elsevier.com/locate/camwa

Lattice Boltzmann simulations of homogeneous isotropic turbulence

Waleed Abdel Kareem [a,*], Seiichiro Izawa [b], Ao-Kui Xiong [c], Yu Fukunishi [b]

[a] *Suez Canal University, Faculty of Science in Suez, Suez, Egypt*
[b] *Graduate School of Engineering, Tohoku University, Japan*
[c] *Wuhan University of Technology, Wuhan, China*

ARTICLE INFO

Keywords:
Lattice Boltzmann
Forced isotropic turbulence
Vortical structures

ABSTRACT

The Lattice Boltzmann Method (LBM) with a forcing scheme is used to simulate homogeneous isotropic turbulence, and the resolutions of 128^3 and 256^3 are compared. Two models, $D3Q15$ and $D3Q19$, are used in the investigation. Results demonstrate that the Lattice Boltzmann Method can capture important features of turbulence such as the vortex-like tubes and the Kolmogorov $-5/3$ power spectrum. Visualization of the elongated vortices using the high rotational identification method, Q, is also presented. For 256^3, a longer range of the Kolmogorov $-5/3$ slope can be observed than in the case of 128^3 grid points. As the resolution increases, the turbulence characteristics of the flow are found to become similar to those obtained in studies by the spectral method regardless of which model is used.

1. Introduction

Direct numerical simulations of homogeneous isotropic turbulence have been studied by numerous researchers such as Vincent and Meneguzzi [1], Kaneda et al. [2] and others. They found that the energy spectrum displays an inertial sub-range, and their visualization of the flow confirmed that the strongest vorticity is organized in very elongated thin tubes. These simulations were performed by using the spectral method to solve the Navier–Stokes equations. Their simulations suggest that the energy spectrum in the inertial subrange almost follows the $k^{-5/3}$ Kolmogorov scaling law where k is the wave number.

Recently, the Lattice Boltzmann method has enabled many researchers to simulate turbulent flow as a new computational tool. Most of these studies concern decaying homogeneous isotropic turbulence [3]. To our knowledge, few studies have investigated forced homogeneous turbulence [4,5] and Cate et al. [6] used a spectral forcing with LBM, where they used the Fourier transformation for the forcing term in each time step.

This paper is organized as follows. In Section 2 we describe the underlying Lattice Boltzmann method and present details of the $D3Q15$ and $D3Q19$ models. In Section 3, we consider the forcing of the flow field and describe the details of the forcing function and the forcing method. The initialization of the flow field is also considered in this section. Section 4 discusses the general characteristics of an isotropic turbulent flow. The turbulent flow length scales are defined as well as the energy spectrum function and the energy dissipation rate. Section 5 is devoted to the results of the study and the discussions of the obtained turbulent features. Section 6 summarizes our conclusions.

* Corresponding author.
E-mail address: waleed_sayed_2000@yahoo.com (W. Abdel Kareem).

0898-1221/$ – see front matter © 2009 Elsevier Ltd. All rights reserved.
doi:10.1016/j.camwa.2009.02.002

2. The Lattice Boltzmann method

The Lattice Boltzmann method has been used widely in simulations of various fluid dynamics problems. See Chen et al. [7] for a review of the Lattice Boltzmann method and the connection with the Navier–Stokes equation. Also, Ubertini et al. [8] and Qi [9] introduced the recent advances of Lattice Boltzmann techniques for fluid-engineering problems.

In this paper, the computation domain is a periodic box of size $L_c = 128^3$ and 256^3. The Bhatnagar–Gross–Krook (BGK) [10] single relaxation time approximation used in the Lattice Boltzmann equation is defined as

$$f_\alpha(\boldsymbol{x} + \boldsymbol{e}_\alpha \delta t, t + \delta t) - f_\alpha(\boldsymbol{x}, t) = \frac{-1}{\tau}(f_\alpha(\boldsymbol{x}, t) - f_\alpha^{eq}(\boldsymbol{x}, t)) + 3\rho w_\alpha(\boldsymbol{e}_\alpha \cdot \boldsymbol{F}), \tag{1}$$

where τ is the single relaxation time and $3\rho w_\alpha(\boldsymbol{e}_\alpha \cdot \boldsymbol{F})$ represents the additional forcing term to the Boltzmann equation (see [11–13]). This implementation of the forcing function can be shown to satisfy the continuity and Navier–Stokes equations up to the second-order [13]. The equilibrium distribution function $f_\alpha^{eq}(\boldsymbol{x}, t)$ is given by

$$f_\alpha(\boldsymbol{x}, t) = w_\alpha \rho \left[1 + 3(\boldsymbol{e}_\alpha.\boldsymbol{u}) + \frac{9}{2}(\boldsymbol{e}_\alpha.\boldsymbol{u})^2 - \frac{3}{2}(\boldsymbol{u}.\boldsymbol{u})\right], \tag{2}$$

where ρ and $\boldsymbol{u}$ are the fluid mass density and velocity.

The weighting coefficients w_α depend on the discrete velocity set $\boldsymbol{e}_\alpha$ and the dimensions of space. In this research, 15-velocity and 19-velocity LBM models on a 3D-cubic lattice are used. The respective discrete velocity sets for the $D3Q15$ and $D3Q19$ models are defined as

$$\boldsymbol{e}_\alpha = \begin{cases} (0,0,0), & (\alpha = 0) \\ (\pm 1,0,0),(0,\pm 1,0),(0,0,\pm 1), & (\alpha = 1-6) \\ (\pm 1,\pm 1,\pm 1), & (\alpha = 7-14), \end{cases}$$

$$\boldsymbol{e}_\alpha = \begin{cases} (0,0,0), & \alpha = 0 \\ (\pm 1,0,0),(0,\pm 1,0),(0,0,\pm 1), & \alpha = 1-6 \\ (\pm 1,\pm 1,0),(\pm 1,0,\pm 1),(0,\pm 1,\pm 1), & \alpha = 7-18. \end{cases}$$

The respective weighting coefficients w_α for the $D3Q15$ and $D3Q19$ models are

$$w_\alpha = \begin{cases} \dfrac{2}{9}, & (\alpha = 0) \\ \dfrac{1}{9}, & (\alpha = 1-6) \\ \dfrac{1}{72}, & (\alpha = 7-14), \end{cases}$$

$$w_\alpha = \begin{cases} \dfrac{1}{3}, & \alpha = 0 \\ \dfrac{1}{18}, & \alpha = 1-6 \\ \dfrac{1}{36}, & \alpha = 7-18. \end{cases}$$

The lattice Boltzmann Method can simulate the Navier–Stokes equations with the viscosity given by

$$\nu = \frac{1}{3}\left(\tau - \frac{1}{2}\right)\delta x, \tag{3}$$

where δx represents the grid spacing.

3. Forcing of the flow field

In order to keep the turbulence in a statistical equilibrium state, a certain amount of energy should be injected into the flow field; otherwise the isotropic turbulence in the box will decay, losing its energy. A turbulent field is numerically forced by injecting energy into the low wave-number Fourier modes.

Forced isotropic turbulence in a periodic box is one of the most basic numerically simulated turbulent flows. Forced isotropic turbulence is achieved by adding energy to the low wave-number modes so that a turbulent cascade develops as statistical equilibrium is reached. Statistical equilibrium is indicated by the balance between the input of kinetic energy through the forcing and its output through the viscous dissipation. There are many methods for forcing homogeneous isotropic turbulent flows. Siggia and Patterson [14] forced their simulations by applying a constant value for the amplitude of the Fourier coefficients in the shell $1 \leq k \leq 2$. Mohseni et al. [15] implemented two different forcing schemes to model the energy injection on larger scales. The first method consists of applying forcing over a spherical shell with walls of unit width

centered at wave-number one, so that total energy injection will be constant with time. The second method corresponds to the forcing used by Chen and Shan [16] where wave modes in a spherical shell $|k| = k_0$ of a certain width are forced in such a way that the forcing spectrum follows Kolmogorov's $-5/3$ scaling law [17].

In this paper, the three components of the forcing term $\boldsymbol{F}$ are defined as

$$\boldsymbol{F} \equiv \begin{cases} F_x = a\left(2\dfrac{k_y k_z}{k^2}\right) G(k_x, k_y, k_z) \\ F_y = -a\left(\dfrac{k_x k_z}{k^2}\right) G(k_x, k_y, k_z) \\ F_z = -a\left(\dfrac{k_x k_y}{k^2}\right) G(k_x, k_y, k_z), \end{cases}$$

and $G(k_x, k_y, k_z)$ is defines as

$$G(k_x, k_y, k_y) = \sin\left(\frac{2\pi x}{L_c}k_x + \frac{2\pi y}{L_c}k_y + \frac{2\pi z}{L_c}k_z + \phi\right) \tag{4}$$

where a and ϕ are the forcing amplitude and the random phase. The forcing is applied to low wave-numbers, $0 < k \leq 2$, where $k = (k_x, k_y, k_z)$ represents the three-dimensional wave number. The forcing takes place every time step to generate a statistical stationary velocity field. The forcing amplitude a for $D3Q15$ simulations is chosen as $a = 10^{-5}$, while $a = 10^{-4}$ is used for the $D3Q19$ model.

It is important to point out some empirical observations of the initialization of the flow field and the forcing amplitude. First, the standard approach to numerically generate isotropic turbulence is to begin from turbulence initialized with Gaussian random numbers conforming to a given initial energy spectrum. In our simulations, the velocity components are set to zero everywhere except at the low wave-numbers $0 \prec k \leq 3$, and the density is set to unity.

Second, when using the $D3Q15$ model, the LBM becomes unstable if a higher amplitude is used. Also, the flow field develops more slowly if a lower amplitude is used. In contrast, the $D3Q19$ simulations are found to be stable and fast when forcing amplitude 10^{-4} is used.

4. Characteristics of the isotropic turbulence

There are three characteristic length scales in an isotropic turbulent flow:

The integral length scale ℓ characterizing the energy containing scales, whose definition is

$$\ell = \frac{3\pi}{4}\frac{\int \frac{E(k)}{k}\mathrm{d}k}{\int E(k)\mathrm{d}k}, \tag{5}$$

where the energy spectrum function $E(k)$ at the scalar wave number $k \equiv (\mathbf{k}\cdot\mathbf{k})^{\frac{1}{2}}$ is defined in spectral space by

$$E(k) = \frac{1}{2}\sum_{k-\frac{1}{2}<|k|\leq k+\frac{1}{2}} |\,\hat{u}^2(k)\,|, \tag{6}$$

and $\hat{u}$ are Fourier coefficients.

The Kolmogorov microscale η is defined as

$$\eta = \left(\frac{\nu^3}{\epsilon}\right)^{\frac{1}{4}}, \tag{7}$$

where ϵ is the averaged energy dissipation rate.

The Taylor microscale λ is defined as

$$\lambda = \sqrt{\frac{15u_{rms}^2}{S_{ij}S_{ij}}}. \tag{8}$$

The energy dissipation rate is defined as follows:

$$\epsilon = 2\nu S_{ij}S_{ij}. \tag{9}$$

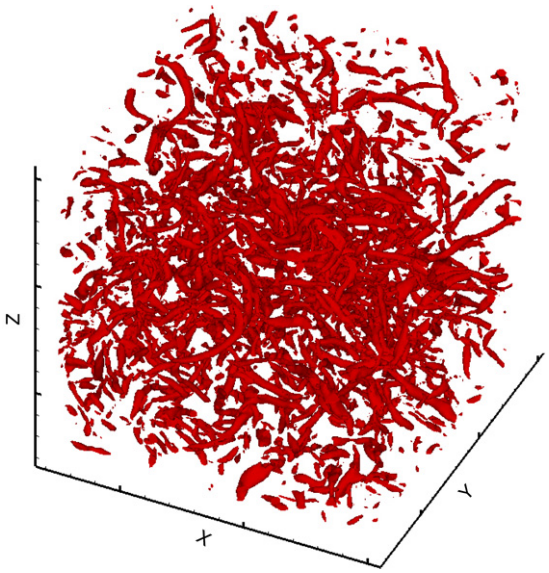

Fig. 1. Isosurfaces of $\frac{Q}{Q_W} = 2.0$ ($D3Q15$,128^3).

5. Results and discussion

Two models of LBM (D3Q15 and D3Q19 models) are compared to evaluate the capability of LBM as a simulation tool for statistically homogeneous isotropic turbulence. The effect of grid resolution is investigated using the $D3Q15$ model, and the results are compared with the spectral method results. The results of this paper can be organized in the following two categories.

(1) **LBM could capture important features of turbulence:**

The Taylor Reynolds number is often used to characterize simulations of forced isotropic turbulence. Several numerical and experimental studies for the same problem using different forcing and initialization of the flow field found that the Taylor Reynolds number for simulations with a resolution of 128^3 is of the order of 100 (e.g., Vincent and Meneguzzi [1]; Kaneda et al. [2]; Jimenez et al. [18]; Comte-Bellot and Corrsin [19] and Ooi et al. [20]). For instance, a study of forced turbulence was performed at a Taylor Reynolds number of 70.9 by Ooi et al. [20]. In the present 128^3 grid point simulations, the Taylor Reynolds numbers $R_\lambda = \frac{u_{rms}\lambda}{\nu}$ based on the Taylor microscale are 55 for the $D3Q15$ model and 72 for the $D3Q19$ model. These values of the Taylor Reynolds number are close to those obtained in the above-mentioned references, and it is within the range $R_\lambda \leq 100$.

The characterization and extraction of vortical structures are considered to be important in understanding the dynamics of turbulent flow fields. Several numerical studies reported that an isotropic turbulent field is filled by tube-like vortices (e.g., Dubief and Declayer [21]; Lesieur and Ossia [22]; Miura and Kida [23]). The presence of worm-like structures in a homogeneous isotropic turbulence has also been confirmed by some experimental investigations (Kuo and Corrsin [24]; Douady and Couder [25]; Cadot et al. [26]; and Villermeaux et al. [27]). The vortical structures for 128^3 are depicted in Figs. 1 and 2 using the high rotational identification method (i.e., the $Q-$identification method) [28]. Here, Q is the second invariant of the velocity gradient tensor and is defined as

$$Q = -\frac{1}{2}(S_{ij}S_{ij} - \Omega_{ij}\Omega_{ij}), \tag{10}$$

where $S_{ij} = \frac{1}{2}(u_{i,j} + u_{j,i})$ and $\Omega_{ij} = \frac{1}{2}(u_{i,j} - u_{j,i})$ are the symmetric and the antisymmetric components of $\nabla\mathbf{u}$. In this paper, Q is normalized by the average enstrophy of the flow field $< Q_W >$. Both models are highly adaptable to this type of flow, though the $D3Q19$ model was more stable than the $D3Q15$ model.

The following discussion only includes the statistical characteristics of the turbulent field for the $D3Q19$ model as it is more robust at higher Reynolds numbers than the $D3Q15$ model. The Taylor (Kolmogorov) microscale is depicted in Fig. 3 (Fig. 4) for the $D3Q19$ model. The Taylor microscale and the Kolmogorov microscale decrease at the beginning of the simulations and both reach a steady state after $t = 150$, where t is the time normalized by the Kolmogorov time. From these results, the flow field is considered to reach a steady state after time step $t = 150$.

(2) **Effect of grid resolution :**

The resolution of small scales, as discussed by Yeung and Pope [29], is characterized by the dimensionless parameter $k_{\max}\eta$. It was claimed that $k_{\max}\eta \geq 1$ is a necessary condition for resolving the small-scale structures. In this paper, we

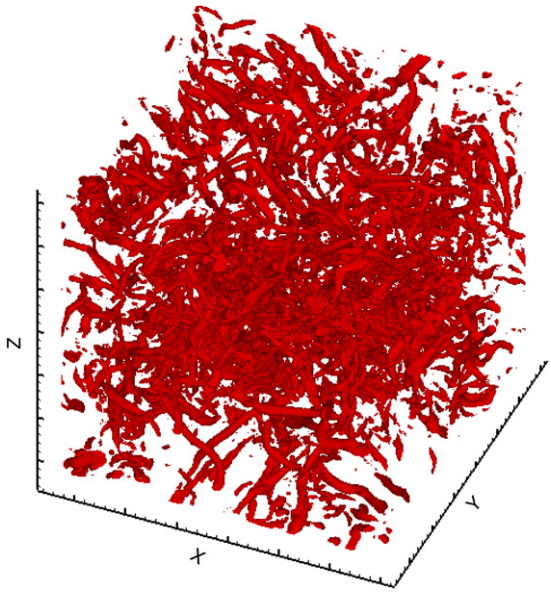

Fig. 2. Isosurfaces of $\frac{Q}{Q_W} = 4.5$ ($D3Q19$,128^3).

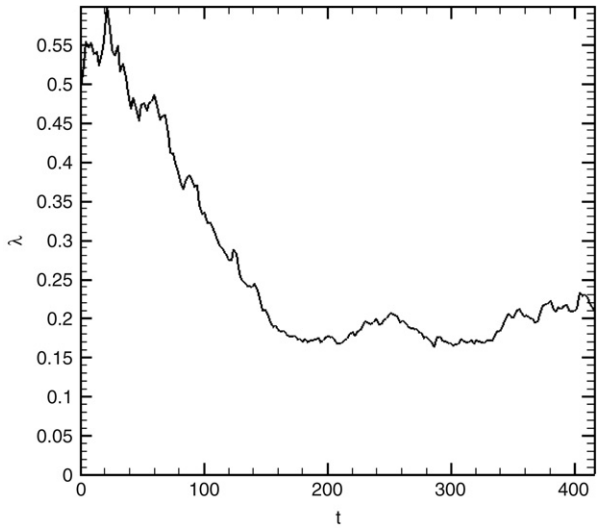

Fig. 3. Evolution of Taylor microscale λ ($D3Q19$, 128^3).

found that $k_{\max}\eta = 1.108$ in the $D3Q19$ simulations, but $k_{\max}\eta = 0.83$ in the $D3Q15$ model. Other characteristics of the turbulent field in both simulations $D3Q15$ and $D3Q19$ compared to the spectral method results are presented in Table 1.

Although the results of the $D3Q19$ model are quite promising and the turbulence characteristics are improved for 128^3 grid points, it may be useful to move to simulations of a higher resolution to test the effect of the grid resolution in such simulations. Simulations with a resolution of 256^3 grid points using the $D3Q15$ model are also tested and compared with the previous results as well as the results obtained by the spectral method. Based on experiment data on grid-generated turbulence (e.g., Comte-Bellot and Corrsin [19]), isotropic turbulence is obtained when spectra begin to collapse at high wave-numbers under Kolmogorov scaling and when the Kolmogorov power law is observed in the inertial sub-range. This scaling can be observed in Fig. 5, which depicts the energy spectrum of the chosen time step $t = 320$ after reaching the steady state. It is clear that the spectrum follows the Kolmogorov $-5/3$ power law. Visualization of the vortical structures is also presented in Fig. 6, where the turbulent field can be observed as groups of fine-scale structures. Comparing Figs. 1 and 6 reveals more fine vortices for 256^3. Statistical properties such as integral length scale, Taylor microscale, and Kolmogorov microscale are very close to those of the spectral method as in Table 2 (series- 1). This means that LBM is a good candidate for simulating this type of fluid flow. These findings suggest that results of the $D3Q15$ model improve as the resolution increases and are similar to those obtained by the spectral method.

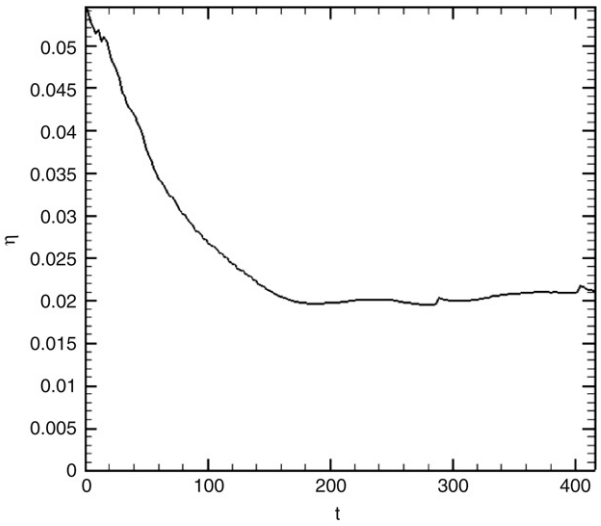

Fig. 4. Evolution of Kolmogorov microscale η ($D3Q19$, 128^3).

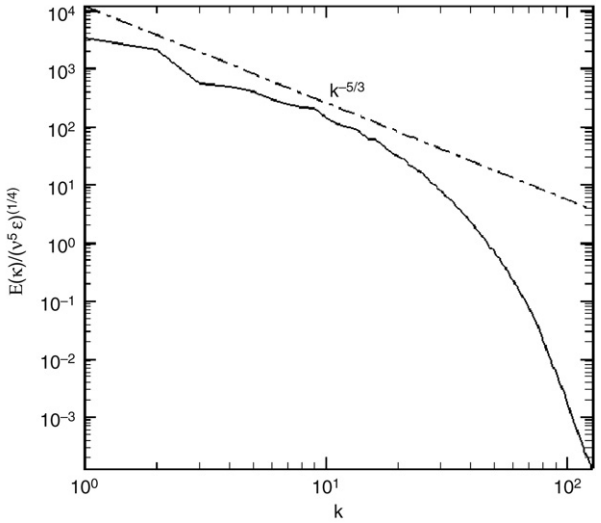

Fig. 5. Energy spectrum of the chosen time step $t = 320$ and the dashed line represents the Kolmogorov power law with a Kolmogorov constant $C_k = 1.8$ ($D3Q15$, 256^3).

Table 1
Characteristics of the turbulent field (Resolution 128^3).

	Present study (D3Q19)	Present study (D3Q15)	Spectral method (SM) [18]
R_λ	72	55	61.1
ℓ	1.67	0.77	1.76
λ	0.2751	0.25	0.5269
η	0.017	0.0125	0.016
$k_{\max}\eta$	1.108	0.83	2.0
$\frac{\ell}{\lambda}$	6.07	3.08	3.34
$\frac{\ell}{\eta}$	103.53	64.2	52

6. Conclusion

Lattice Boltzmann simulations of forced isotropic turbulence were performed successfully with resolutions of 128^3 and 256^3. It was demonstrated that the Lattice Boltzmann method could capture important features of turbulence. It was also demonstrated that the energy spectrum, turbulent length scales and vortical structures of the turbulent flow field are in good agreement with results of previous studies obtained by the spectral method. As the resolution of the simulation increases, the turbulence statistical characteristics were found to become similar to results obtained by the spectral method regardless

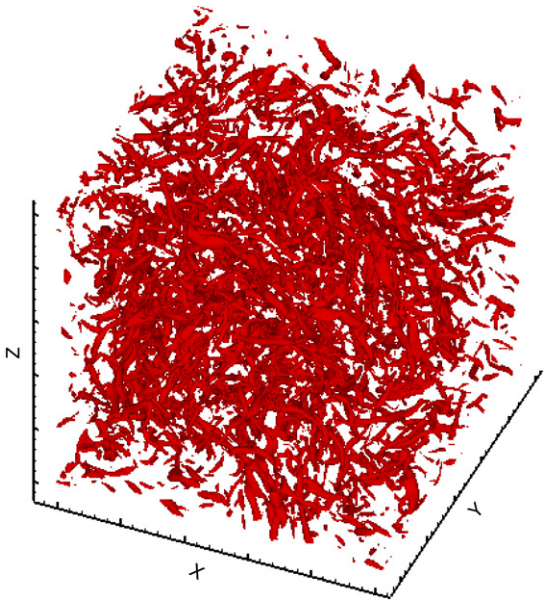

Fig. 6. Isosurfaces of $\frac{Q}{Q_W} = 5.981$ ($D3Q15, 256^3$).

Table 2
Characteristics of the turbulent field ($D3Q15$ model, 256^3).

	Present study	SM [2] (series-1)	SM [2] (series-2)
R_λ	180	167	94
ℓ	1.0058	1.13	1.10
λ	0.2539	0.203	0.326
η	0.0096	0.007	0.017
$k_{\max}\eta$	1.2288	0.847	2.057
$\frac{\ell}{\lambda}$	3.96	5.57	3.37
$\frac{\ell}{\eta}$	104.8	161.43	64.71

of which model is used. This research supports previous studies about the capability of the Lattice Boltzmann method to simulate complex flows.

References

[1] A. Vincent, M. Meneguzzi, J. Fluid Mech. 225 (1991) 1–20.
[2] Y. Kaneda, T. Ishihara, M. Yokokawa, K. Itakura, A. Uno, Phys. Fluids 15 (2003) L21–L24.
[3] H. Yu, S. Girimaji, L.-S. Luo, Phys. Rev. E 71 (2005) 016708.
[4] W. Abdel Kareem, Ph.D. Thesis, Tohoku Univesity, Japan, 2006.
[5] W. Abdel Kareem, S. Izawa, A.K. Xiong, Y. Fukunishi, J. Turbulence 8 (N12) (2007) 1–15.
[6] A. Cate, E. Vilet, J. Derksen, H. Van en Akker, Comput. & Fluids 35 (2006) 1239–1251.
[7] S. Chen, G. Doolen, Annu. Rev. Fluid Mech. 30 (1998) 329–364.
[8] S. Ubertini, S. Succi, Prog. Comput. Fluid Dyn. 5 (2005) 85–96.
[9] D. Qi, Prog. Comput. Fluid Dyn. 5 (2005) 104–109.
[10] P. Bhatnagar, E. Gross, M. Krook, Phys. Rev. 94 (1954) 511–525.
[11] S. Succi, The Lattice Boltzmann Equation for Fluid Dynamics an Beyond, Oxford University Press, 2001.
[12] J.A. Cosgrove, J.M. Buick, S.J. Tonge, C.G. Munro, C.A. Greated, D.M. Campbell, J. Phys. A: Math. Gen. 36 (2003) 2609–2620.
[13] J. Buick, C. Greated, Phys. Rev. E 61 (2000) 5307–5320.
[14] E. Siggia, G. Patterson, J. Fluid Mech. 86 (1987) 567–592.
[15] K. Mohseni, B. Kosovic, S. Shkoller, J. Marsden, Phys. Fluids 15 (2003) 524–544.
[16] S. Chen, X. Shan, Comput. Phys. 6 (1992) 643–646.
[17] A.N. Kolmogorov, Dokl. Akad. Nauk SSSR 30 (1941) 9–13.
[18] J. Jimenez, A. Wray, P. Saffman, R. Rogallo, J. Fluid Mech. 255 (1993) 65–90.
[19] G. Comte-Bellot, S. Corrsin, J. Fluid Mech. 48 (1971) 273–337.
[20] A. Ooi, J. Martin, J. Soria, M. Chong, J. Fluid Mech. 381 (1999) 141–174.
[21] Y. Dubief, F. Declayre, J. Turbulence 1 (N11) (2000).
[22] M. Lesieur, S. Ossia, J. Turbulence 1 (N7) (2000).
[23] H. Miura, S. Kida, J. Phys. Soc. Japan 66 (1997) 1331–1334.
[24] A. Kuo, S. Corrsin, J. Fluid Mech. 56 (1972) 447–479.
[25] S. Douady, Y. Couder, P. Barchet, Phys. Rev. Lett. 67 (1991) 983–986.
[26] O. Cadot, S. Douady, Y. Couder, Phys. Fluids 7 (1995) 630–634.
[27] E. Villermaux, B. Sixou, Y. Gene, Phys. Fluids 7 (1995) 2008–2013.
[28] J. Hunt, A. Wray, P. Moin, Report CTR-S88, Center for Turbulence Research, 1988, pp. 193–208.
[29] P. Yeung, S. Pope, J. Fluid Mech. 207 (1989) 531–586.